Plasmonic gold-embedded TiO_2 thin films as photocatalytic self-cleaning coatings

Plasmonic gold-embedded TiO$_2$ thin films

as photocatalytic self-cleaning coatings

Hannelore Peeters[1], Maarten Keulemans[1], Gert Nuyts[2], Frederik Vanmeert[2], Chen Li[3], Matthias

Minjauw[4], Christophe Detavernier[4], Sara Bals[3], Silvia Lenaerts[1], Sammy W. Verbruggen[1*]

[1] Sustainable Energy, Air & Water Technology (DuEL), Department of Bioscience Engineering, University of Antwerp, Groenenborgerlaan 171, 2020 Antwerp, Belgium.

[2] Antwerp X-ray analysis, Electrochemistry and Speciation (AXES), Department of Chemistry, University of Antwerp, Groenenborgerlaan 171, 2020 Antwerp, Belgium.

[3] Electron Microscopy for Materials Science (EMAT), Department of Physics, University of Antwerp, Groenenborgerlaan 171, 2020 Antwerp, Belgium.

[4] Conformal Coating of Nanomaterials (COCOON), Department of Solid state sciences, Gent University, Krijgslaan 281 S12, 9000 Gent, Belgium

*Corresponding author: Sammy.Verbruggen@uantwerpen.be

1 **Abstract**

2 Transparent photocatalytic TiO_2 thin films hold great potential in the development of self-cleaning

3 glass surfaces, but suffer from a poor visible light response that hinders the application under actual

4 sunlight. To alleviate this problem, the photocatalytic film can be modified with plasmonic

5 nanoparticles that interact very effectively with visible light. Since the plasmonic effect is strongly

6 concentrated in the near surroundings of the nanoparticle surface, an approach is presented to embed

7 the plasmonic nanostructures in the TiO_2 matrix itself, rather than deposit them loosely on the surface.

8 This way the interaction interface is maximised and the plasmonic effect can be fully exploited. In this

9 study, pre-fabricated gold nanoparticles are made compatible with the organic medium of a TiO_2 sol-

10 gel coating suspension, resulting in a one-pot coating suspension. After spin coating, homogeneous,

11 smooth, highly transparent and photoactive gold-embedded anatase thin films are obtained.

12

15

1. Introduction

When TiO_2 is used in self-cleaning applications, it is usually deposited as a thin film that is capable of removing pollutants from the surface using (sun)light. The film thickness typically ranges from a few nanometres to several micrometres.[1–3] TiO_2 thin films can be deposited by a wide variety of methods, ranging from target sputtering over sol-gel deposition, thermal methods, vapour deposition techniques (PVD/CVD/ALD), anodic oxidation and plasma-assisted deposition processes.[4–11] In this work, the sol-gel method is selected because it is straightforward, affordable and it can be applied directly onto a wide variety of substrates using easy and low-cost techniques such as spin or dip coating.[3] Furthermore, this simple yet versatile sol-gel process is an ideal method to obtain thin film coatings of high transparency, which is a crucial parameter when applying self-cleaning films onto glass surfaces. One of the main constraints of photocatalytic self-cleaning materials on the market, is their limited solar-light response. Photocatalytic films based on unmodified TiO_2 as the active ingredient are only activated by the UV-component of solar light, and thus only ca. 4-5% of the incident solar light spectrum is actually used effectively. [12,13]

To further improve the photocatalytic self-cleaning activity under solar light, we propose to modify the films by plasmonic nanoparticles embedded in the active layer. Surface plasmon resonance (SPR) is induced by incidence of photons of a resonant wavelength, which results in the collective oscillation of free electrons in the conduction band. This unique optical property of (noble) metal nanoparticles allows the concentration and manipulation of light at the nanoscale, which has resulted in different applications such as sensors, energy production, surface enhanced Raman spectroscopy and photocatalytic environmental remediation. [12,14] In contrast to traditional methods, where modification with plasmonic nanoparticles occurs by simply mixing, depositing or (photo-) impregnating them on the surface of the photocatalyst in a *multi*-step process,[15–22] here, the nanoparticles are first stabilised and mixed with the titanium precursor sol. Hence, this procedure provides a 'one-pot' coating suspension that can be readily applied. This is expected to facilitate a

3

1   homogeneous dispersion and stable embedment of the plasmonic nanoparticles throughout the

2   resulting TiO_2 matrix. The additional advantage of fully embedding the nanoparticles into the

3   photocatalytic TiO_2 film can be rationalised as follows: (i) under UV light irradiation electron-hole pairs

4   are generated in the TiO_2 semiconductor, while the metal nanoparticles solely act as passive electron

5   sinks, resulting in less recombination events.[23] (ii) On the other hand, previous research has also

6   shown that for Au/TiO_2 composites under visible light illumination, direct "hot electron" injection from

7   the excited plasmonic nanoparticles into the conduction band of TiO_2 plays an important role,[24,25]

8   as well as an increase of the electromagnetic near-field within a 3 nm radius surrounding the plasmonic

9   nanoparticle, as investigated by Asapu *et al.*[26,27] Regardless of the excitation wavelength,

10 maximising the direct contact interface between the nanoparticle and the semiconductor is of

11 paramount importance for both of these electron and energy transfer processes. As a consequence,

12 by partially or fully embedding the nanoparticles in the TiO_2 matrix, the contact interface is increased

13 substantially and may lead to considerably higher photocatalytic activities (Figure 1).[28,29] In

14 addition, partially or fully embedding the nanoparticles in a rigid matrix is hypothesised to protect

15 them from chemical corrosion, reshaping, agglomeration and detachment during post-treatment or

16 photocatalytic testing, thereby adding to the stability of the entire composite system.[30,31]
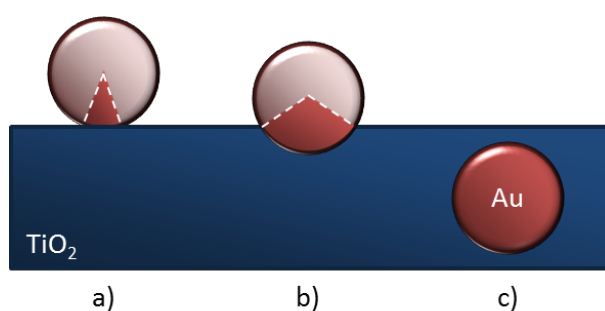
17

18 **Figure 1.** Schematic representation of the interfacial area through which charge transfer between the metallic nanoparticle

19 and semiconductor can take place when (a) the nanoparticle is atop the semiconductor, (b) partially embedded and (c) fully

20 embedded in the TiO_2 matrix.

4

1   A vast amount of literature can be found on several synthesis procedures enabling the preparation

2   of nanoparticles of different compositions, shapes and sizes, whether or not functionalised with

3   specific ligands. In the proposed approach, the plasmonic metal nanoparticles are first prepared

4   separately after which they are introduced in the sol-gel precursor solution ("*ex-situ"* method). This

5   entails several advantages over an "*in-situ*" approach, where a metal salt precursor and TiO_2 precursor

6   are mixed, simultaneously forming metal nanoparticles and TiO_2.[32–35] In other words, the *ex-situ*

7   method enables much more accurate and precise control over the nanoparticle properties, tailored to

8   the envisaged application.[36] *In-situ* synthesis procedures on the other hand only enable limited

9   control over the nucleation process and final nanoparticle size and shape.[33] The only difficulty that

10   lies in the proposed strategy is that the plasmonic metal nanoparticles (typically prepared in an

11   aqueous medium) have to be made compatible with the titania precursor coating sol (typically organic

12   solvent based). One possible solution to this problem is proposed by Sonawane et al. [37] It involves

13   complete condensation of a Ti-alkoxide precursor followed by re-dissolution in aqueous hydrogen

14   peroxide to render it compatible with the aqueous nanoparticle colloids. In our work, the use of such

15   harsh conditions is avoided by achieving the opposite: adapting the colloids to the coating sol. A similar

16   strategy has been investigated by the group of Mulvaney, with the eye on gas-sensing applications.[33]

17   The metal loadings used in that particular study are, however, quite high (ranging from 4 to 8 wt%)

18   and no photocatalytic activity data have been collected. In the present work, thin TiO_2 films are

19   modified with gold nanoparticles up to 3 wt% loading. The resulting effect on transparency is evaluated

20   and the photocatalytic activity is measured by means of stearic acid degradation under simulated solar

21   light, with the eye on real outdoor applications. This is a widely recognised model reaction as stearic

22   acid is a representative of the group of organic fouling compounds that typically contaminate glass

23   surfaces.[1,5,38] This study thus goes beyond the state-of-the-art of (photocatalytic) self-cleaning

24   surfaces in that sense that currently commercially available photocatalytic self-cleaning materials can

25   only utilise the UV-component of solar light. The goal is to expand the activity window towards the

1 entire solar spectrum. This would not only increase the efficiency for outdoor use, but could also

2 enable the use of such surfaces under artificial (indoor) light.

3 **2. Methodology**

4 ***PVP stabilised gold nanoparticle synthesis***

5 Aqueous colloidal suspensions of Au nanoparticles were prepared using a modified Turkevich

6 procedure [39] as described previously [20,40], but in a ten times higher concentration. In short, 10 mL

7 of a 0.01 M $HAuCl_4.3H_2O$ (Sigma-Aldrich, >99.9%) was diluted so a total metal concentration of 1 mM

8 was obtained in the final reaction volume. The solution was stirred vigorously and brought to boil after

9 which 10 mL of a freshly prepared 1 wt% sodium citrate (Sigma-Aldrich, 99%) solution that acts as both

10 the stabiliser and the reducing agent, was quickly added. After exactly 30 minutes of boiling, the

11 resulting colloidal Au suspension was immediately cooled to room temperature.

12 A phase transfer of the nanoparticles from the aqueous phase to the organic phase is achieved

13 by exchanging the sodium citrate with PVP (polyvinylpyrrolidone, Alfa Aesar, 10000 g mol^{-1}). PVP was

14 dissolved in water by ultrasonication (45 kHz) for 15 minutes. An appropriate amount of the PVP

15 solution (2.5 mM) was added to the colloidal Au suspension so that 60 PVP molecules were provided

16 per nm² nanoparticle surface. The solution was stirred at 600 rpm for 24 h at room temperature to

17 ensure complete exchange of the stabilising agent.[41] The resulting PVP stabilised Au nanoparticles

18 were finally centrifuged at 9000 rpm for 20 minutes, washed and re-suspended in absolute ethanol

19 (Emplura, 99.5%). UV-VIS absorption spectra of the colloidal Au nanoparticle solutions were measured

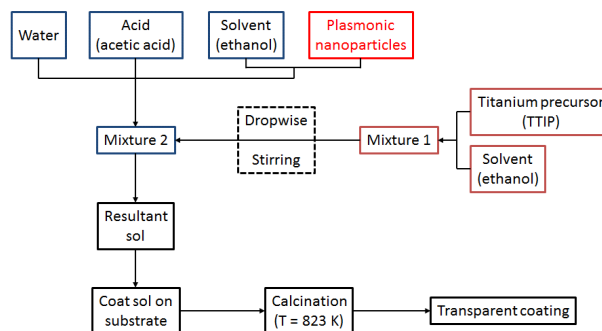20 with a Shimadzu UV-VIS 2600 double beam spectrometer.

21 ***Preparation of plasmon modified thin films***

22 For the substrate preparation, low p-doped silicon wafers (15 mm x 30 mm) were cleaned

23 ultrasonically in methanol and blown dry with compressed air. Borosilicate glass was used as glass

1 substrates (15 mm x 30 mm, Borofloat® 33) after cleaning for 15 min at room temperature in fresh

2 piranha solution (7:3 v/v sulfuric acid (Chem-Lab, 95-97%):hydrogen peroxide (Chem-Lab, 30%)) and

3 rinsing three times with bi-distilled water. The cleaned glass slides were stored in bi-distilled water and

4 blown dry with compressed air just before spin-coating.

5   The (modified) titania sols were prepared by the hydrolysis of titanium(IV)isopropoxide (TTIP,

6 Sigma-Aldrich, 97%) in the presence of acetic acid (Riedel-de Haën, 96%). A solution of TTIP and ethanol

7 (0.05:1.64 molar ratio) (henceforth referred to as Mixture 1) was added dropwise (average drop

8 volume 0.021 ± 0.005 mL over 200 s) to a solution containing water, ethanol and acetic acid

9 (1.07:1.31:0.34 molar ratio) (referred to as Mixture 2) under vigorous stirring. In the case of Au/TiO_2

10 thin film preparation, the ethanol part of Mixture 2 was replaced by a concentrated dispersion

11 containing appropriate amounts of gold nanoparticles in ethanol. The exact concentration of the added

12 Au NPs colloidal suspension was determined quantitatively using Spectroquant® analysis (NOVA 60,

13 Merck) using a standard gold test kit (114 821). This way, sols were prepared with a nominal and actual

14 gold loading of 0.1, 0.3, 0.5, 1 and 3 wt% (calculated and measured relative to the total amount of

15 TiO_2). The viscosity change of the formed sol was monitored with a Brookfield LVDV-I prime Digital

16 Viscometer operated at a spindle speed of 12 rpm, to ensure all samples were spin coated at the same

17 viscosity. Film deposition was achieved by spin coating both the glass and silicon substrates at 1000

18 rpm for one minute at room temperature. Finally, the samples were calcined at 823 K for three hours

19 at a heating rate of 1 K min^{-1}. The overall synthesis procedure is schematised in Figure 2.

Figure 2. Schematic representation of the used ex-situ synthesis procedure (nanoparticle synthesis is separated from sol-gel process) to obtain plasmon modified transparent thin films.

To evaluate the proposed procedure, it was compared with Sonawane's sol-gel procedure. The sol-gels were prepared as reported by Sonawane *et al.* [32]. For the plasmon modified sol-gels, prefabricated non-PVP exchanged Au nanoparticles were used. Once the sol-gel had aged to the right viscosity, it was spin-coated onto clean silicon wafers and borosilicate substrates as previously described.

Characterisation of plasmon modified thin films

Film thickness of the samples was measured using a J.A. Woollam M-2000 spectroscopic ellipsometer working in the UV-VIS spectrum. The data were fitted using the standard Cauchy model with CompleteEASE software. The optical model consisted of a substrate with the titania coating on top, parametrised with the Cauchy dispersion relation to fit the film thicknesses.

To confirm the crystal structure of TiO_2 formed during calcination, X-ray diffraction (XRD) patterns were measured with a Cu-tube (IuS-Cu[HB], Incoatec) with a potential of 50 kV, a current of 1 mA and a 2D detector (PILATUS200K, Dectris). The averaged signal comes from the titania coating scraped off a silicon wafer, measured for 38 min.

A Shimadzu UV-VIS 2501PC double beam spectrophotometer was used to measure the UV-VIS absorption spectra of the calcined titania films with different weight loadings of gold.

1   The transparency of the coatings was evaluated by measuring the loss in total integrated

2   transmittance of combined simulated solar light (300 W Xe source (Oriel Instruments) equipped with

3   an AM1.5 solar simulator, incident intensity of 100 mW cm^{-2}) passing through the coated films and

4   comparing this to unmodified Borofloat® as well as a commercial benchmark PilkingtonActiv™. The

5   total integrated transmittance was measured directly at the sample with a calibrated Intensity

6   spectrometer (Avantes Avaspec 3648).

7   The smoothness of the thin films on Borofloat® was verified by Atomic Force Microscopy (AFM)

8   using a Bruker Dimension Edge system and compared to uncoated Borofloat® as well as a commercial

9   benchmark PilkingtonActiv™.

10   Original surfaces and in liquid nitrogen cryofractured cross-sections of Borofloat® samples were

11   analysed by a Field Emission Gun – Environmental Scanning Electron Microscope (FEG-ESEM) equipped

12   with an Energy Dispersive X-Ray (EDX) detector (FEI Quanta 250), using an accelerating voltage of 10-

13   20 kV. All samples were coated with 20 nm of carbon prior to SEM-EDX analysis. A beam current of

14   ~0.5 nA was used for the acquisition of backscattered electron (BE) images as well as EDX line scans.

15   All EDX data analyses were performed by using the Aztec software package (Oxford Instruments).

16   The TiO$_2$ film with embedded Au NPs was also spin-coated onto a Mo transmission electron

17   microscopy (TEM) grid with a carbon film that underwent the same procedure as the other sol-gel

18   coated substrates. An FEI Osiris electron microscope in the scanning transmission electron microscopy

19   (STEM) mode was employed to image the sample using a high-angle annular dark-field (HAADF)

20   detector at 200 kV. A Fischione tomography holder (model 2020) with a tilt range of ± 79.5° was used

21   to tilt the TiO$_2$ film allowing the observation of the cross-section and even underneath the film.

22   Water contact angle measurements with an Ossila contact angle goniometer and accompanying

23   Ossila Contact Angle Measurement Software provided data on the wettability of the coatings. The

24   angle of a drop of 4 µL deionised water was recorded at 5 frames per second for 15 seconds of which

1 the last 2 seconds were used to analyse and average the equilibrated water contact angle. To study

2 light-induced effects on hydrophilicity, these measurements were repeated under UVA irradiation

3 (λ_{max} = 350 nm, provided by a fluorescent lamp, Philips Cleo 25 W, incident intensity of 6.9 mW cm^{-2}).

4 ***Evaluation of the self-cleaning activity***

5 The photocatalytic self-cleaning test was conducted by means of a stearic acid degradation

6 experiment, based on the method proposed by Paz *et al*.[1] In short, a layer of stearic acid was applied

7 on top of the prepared thin films on the silicon wafers by spin coating 100 μL of a 0.25 wt% solution of

8 stearic acid (Sigma-Aldrich, >98.5%) in chloroform (Sigma-Aldrich, >99.8%) at 1000 rpm for one minute.

9 The resulting sample was dried at 363 K and subsequently allowed to equilibrate in the test

10 environment for one hour. During the photocatalytic experiments, the samples were illuminated with:

11 combined simulated solar light (300 W Xe source (Oriel Instruments) equipped with an AM1.5 solar

12 simulator, incident intensity of 100 mW cm^{-2}) or UVA light (λ_{max} = 350 nm, provided by a fluorescent

13 lamp, Philips Cleo 25 W, incident intensity of 6.9 mW cm^{-2}). The corresponding irradiance spectra are

14 given in Supporting Information Figure S1. Incident light intensity, photon fluxes and transmission

15 measurements were performed with a calibrated intensity spectrometer (Avantes Avaspec 3648). The

16 remaining surface coverage of stearic acid was measured using a Nicolet^{TM} 380 (Thermo Fisher

17 Scientific) FTIR spectrophotometer equipped with ZnSe windows. All spectra were recorded in the

18 wavenumber range 400-4000 cm^{-1} at a resolution of 2 cm^{-1}. For each measurement, eight spectra were

19 averaged. The samples were placed at a fixed angel of 9° with the IR beam in order to minimise internal

20 reflections. The stearic acid concentration is related to the integrated absorbance in the wavenumber

21 range 2800-3000 cm^{-1}, so that one unit of integrated area (in a.u. cm^{-1}) corresponds to 1.39 x 10^{16}

22 stearic acid molecules cm^{-2} as determined by a pre-established calibration curve (R^2 = 0.99).[20] The

23 initial stearic acid concentration in the experiments was typically around 9 x 10^{15} molecules cm^{-2}.

24

3. Results and Discussion

PVP stabilised gold nanoparticles

Concentrated, aqueous gold suspensions were prepared based on the Turkevich method. The resulting colloidal solutions were dark red and showed a similar UV-VIS absorption spectrum to the 100% Au suspensions described in earlier work, indicating that increasing the concentration has no effect on the final nanoparticle properties.[20,40] Transmission electron microscopy (TEM) confirmed that Au nanoparticles with a mean diameter of (16 ± 4) nm are obtained with this method (Figure S4). An important step in the synthesis procedure described in Figure 2 is the proper stabilisation of the nanoparticles, so they can be used at high concentrations in an organic solvent. Sodium citrate only weakly stabilises the nanoparticles causing them to agglomerate in the presence of an organic solvent, thus a phase transfer step is required.[41–43] To achieve this, the sodium citrate was exchanged with PVP, as PVP stabilised nanoparticles are considerably more stable in organic media.[42,43] The effect of this exchange on the UV-VIS absorption spectrum can be observed in Figure 3. After ligand exchange, a small red shift of the plasmon peak is detected. This is in line with results obtained by Bastús *et al*., who observed a similar red shift after ligand exchange with various surfactants.[44] This shift is ascribed to an increase in the hydrodynamic diameter (*i.e.* including coating material and solvation layer), caused by capping the nanoparticles with a bigger, bulky molecule like PVP.
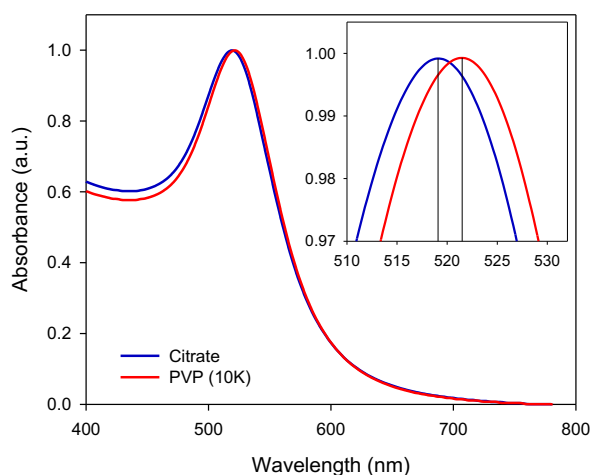
1

2 **Figure 3.** Normalised UV-VIS absorption spectra of the colloidal gold nanoparticle suspensions before (blue curve) and after

3 (red curve) ligand exchange. In the inset, a small red shift of the absorption peak is apparent.

4 **Coating characteristics**

5 The PVP stabilised nanoparticles were dispersed in ethanol and added to Mixture 2 to be

6 incorporated into the TiO_2 matrix during the sol-gel process (Figure 2). Thin films were deposited on

7 both silicon wafers and glass substrates by spin-coating the resulting sols at the same viscosity.

8 Moderate variations in the coating sol viscosity show a negligible effect on the resulting film thickness

9 that was determined by means of ellipsometry and amounted to (78 ± 3) nm on silicon wafers and (55

10 ± 5) nm on glass substrates when spin coated at a spinning speed of 1500 rpm (Figure 4a). Altering the

11 spinning speed, on the other hand, obviously affects the resulting film thickness to a large extent

12 (Figure 4b). Based on these results, a spin-coating speed of 1000 rpm was selected for the plasmon

13 modified thin films, resulting in a layer thickness of 94 nm (Figure 4b, red circle).
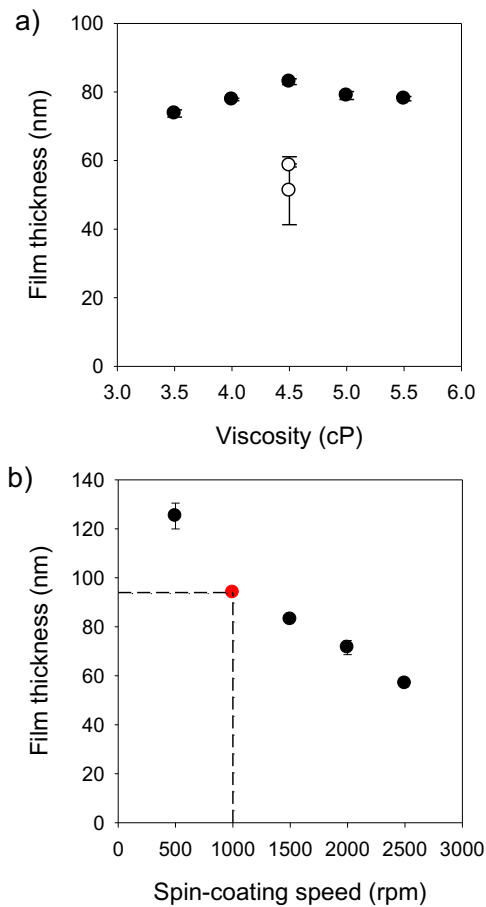
Figure 4. Effect of (a) viscosity (spin-coated at 1500 rpm) and (b) spin-coating speed (viscosity fixed at 4.5 cP) on resulting film thickness. Filled circles correspond to silicon wafer substrates, open circles to glass substrates.

XRD spectra (Figure S2 in Supporting Information) confirm that the obtained crystal structure of the TiO$_2$ thin film is anatase as expected based on the applied calcination temperature. [45] It is expected that the organic PVP shell surrounding the gold nanoparticles is effectively removed upon oxidative calcination at 500°C, similar to what has even been observed for thick carbonaceous layers covered by TiO$_2$ thin films that were subjected to the same treatment. [46]

The absorption spectra of the final calcined TiO$_2$ films with embedded Au nanoparticles at incremental weight loadings up to 3 wt% show a clear red shift of the SPR band from 521.5 nm (colloidal suspension of PVP stabilised Au nanoparticles, Figure 3) to 626 nm for the embedded Au in TiO$_2$ films, Figure 5. This is a common effect that can be attributed to the higher refractive index of the

1   surrounding medium (TiO_2 instead of water).[33] Since the Au nanoparticles are expected to be largely

2   embedded in the TiO_2 matrix itself, the observed red shift is also considerably larger (Δ = 104.5 nm)

3   compared to the one observed in earlier work, where the nanoparticles were only deposited on the

4   TiO_2 surface and thus mostly surrounded by air as the dielectric medium (Δ = 24 nm). [20,40] For the

5   0.1 wt% Au sample, no clear plasmon band could be observed. For the remaining metal loadings, the

6   plasmon band becomes more apparent as the metal loading increases. No obvious broadening of the

7   plasmon band, nor shift of the peak maximum is observed after introducing higher metal loadings,

8   indicating the Au nanoparticles remain well dispersed and do not cluster in the TiO_2 matrix, as will be

9   confirmed by SEM and TEM analysis further down this work.
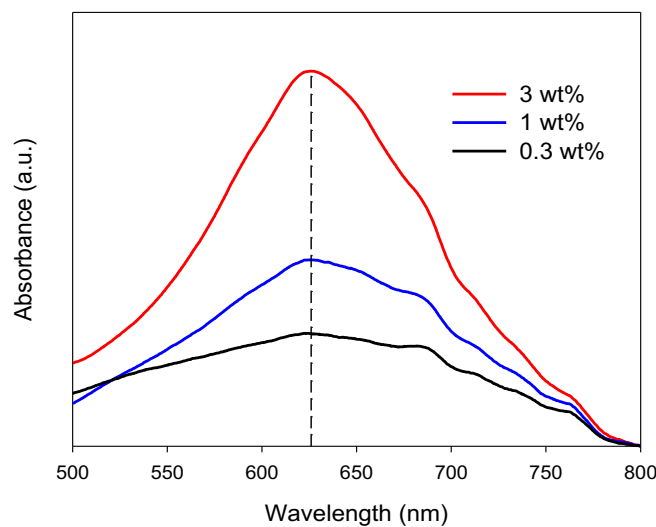
11 **Figure 5:** Absorption spectra of the Au modified thin films with different loadings on glass calcined at 823 K. The dashed

12 vertical line indicates the SPR band maximum at 626 nm.

13   In view of potential commercial applications, it is important to obtain transparent, solar light

14   active films. The transparency of the coatings is therefore evaluated by measuring the relative loss in

15   total integrated transmittance of AM1.5 simulated solar light passing through the coated films, relative

16   to unmodified borosilicate glass (Figure 6a). Coating the glass slide with a thin, unmodified layer of

17   TiO_2 reduces the overall transmittance of the sample by only 14%. Macroscopically, this can hardly be

18   observed by the naked eye; only a slight colour difference of the coated glass is noticeable. At this

point, no actions have been undertaken to further improve the transparency of the TiO_2 film if needed. Lowering the film thickness could for instance already improve the transparency, but a trade-off with photocatalytic activity should be kept in mind. Combining TiO_2 with a low refractive index material like SiO_2 is another method that allows to control the optical properties of the resulting film.[3,47] However, this is outside the scope of the present study. Commercially available photocatalytic self-cleaning glass, PilkingtonActiv[TM], has a 13% transmittance reduction, indicating that a loss in transmittance of 14% is perfectly acceptable for the pure TiO_2-coating in view of real applications. Embedment of stabilised plasmonic nanoparticles in the TiO_2 matrix up to 1 wt% induces no additional loss in transparency. For the highest metal loading of 3 wt%, a negligible additional loss in transparency of 1% with regard to the unmodified TiO_2 film is measured. This is a promising result as it indicates that adding gold nanoparticles only has a limited effect on the light transmitting properties of the resulting films. A photograph of the overall macroscopic appearance of the coated films is presented in Figure 6 b.
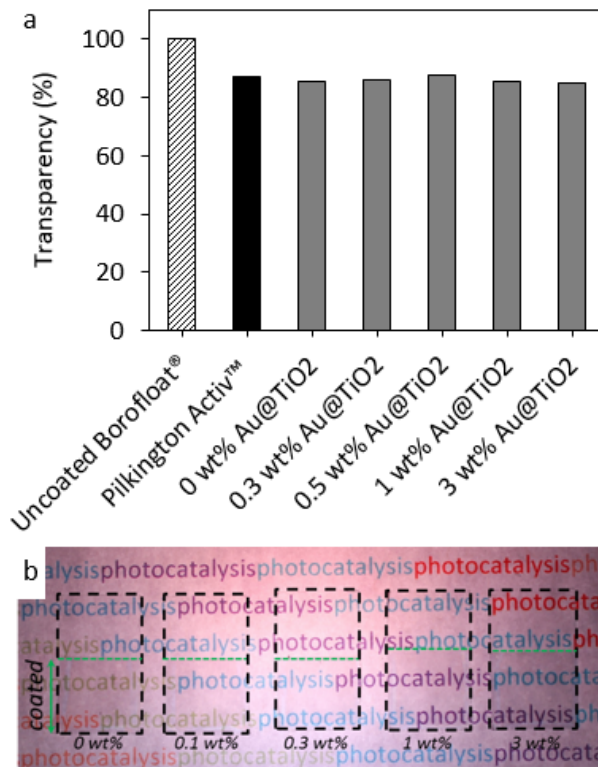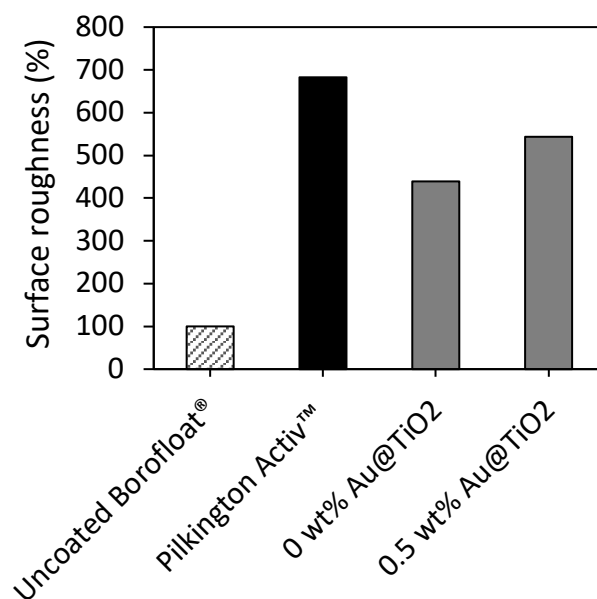
Figure 6. a) Transparency relative to uncoated glass (dashed bar, set at 100%), for commercially available TiO_2-based self-cleaning glass PilkingtonActiv™ (black bar) and the newly developed coatings containing varying stabilised plasmonic Au weight loadings from 0 – 3 wt% (grey bars); b) Photograph of the (half-)coated glass slides. Only the zone underneath the green dashed lines is coated for easy comparison purposes. The photograph is taken by arranging the slides on a paper sheet with the word 'photocatalysis' printed in multiple colours, that is deposited on the cover plate of a 30 W Flood Light LED projector (TDII) set to the 'white light' modus.

The average roughness factor (R_a) of the coatings was determined by AFM measurements and shows that a bare Borofloat® glass substrate has R_a = 0.23 nm. The pure TiO_2 sample prepared with the newly proposed method has R_a = 1.01 nm, which is smoother than the commercial benchmark PilkingtonActiv™ with R_a = 1.57 nm. The plasmon-embedded thin films with a gold loading of 0.5 wt% of Au NPs result in thin films with an R_a of 1.25 nm. When the surface roughness of the different coated substrates is plotted relative to uncoated Borofloat® (Figure 7), it is clear that, even though the samples are 4 to 5 times rougher compared to bare Borofloat®, they are still much smoother than commercially available self-cleaning glass.

1

Figure 7. Surface roughness relative to uncoated glass (dashed bar, set at 100 %), for commercially available TiO_2-based self-cleaning glass PilkingtonActiv™ (black bar) and the newly developed coatings with pure titania and with 0.5 wt% stabilised plasmonic Au in titania (grey bars).

The coating was investigated by backscattered electron imaging of cryofractured cross sections and top views of coated silicon and Borofloat® substrates. The actual coating could not be visualised in the cross-sections, because it was too thin to be clearly observed by SEM, although EDX measurements on the edge of the fractured substrates clearly show the presence of a thin Ti-containing layer (Figure S3). On the BE image of the top view of the coated Borofloat®, homogeneously distributed small bright spots are visible corresponding to the Au NPs (Figure 8 a). It is important to mention that under the given experimental conditions the entire depth of the TiO_2 layer is visualised by means of BE imaging. The difference in brightness thus points at different degrees of embedment of the NPs in the TiO_2 layer.
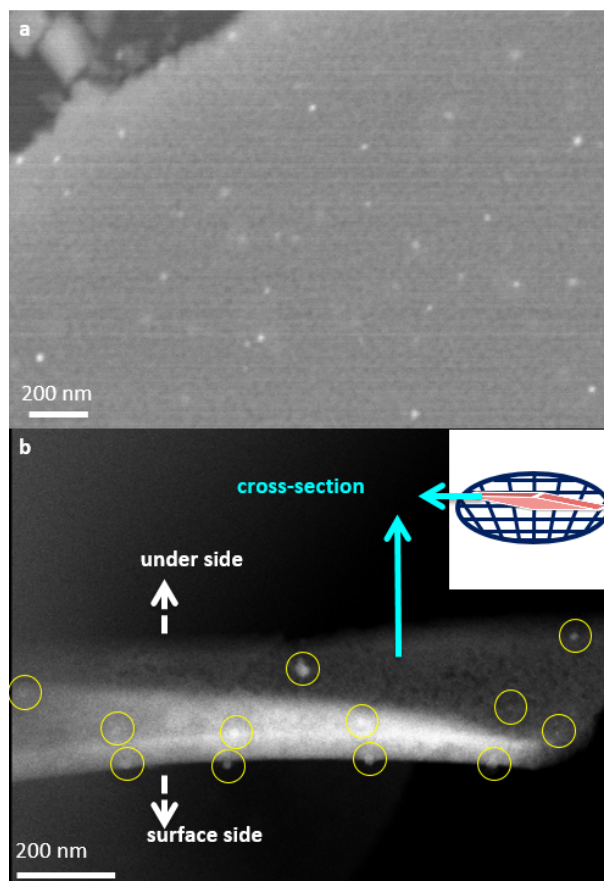
Figure 8: a) Top view of 0.5 w% Au TiO$_2$ coating on Borofloat® visualised with SEM at 10 kV and 100 000 times enlarged; b) STEM-ADF image showing the distribution of Au NPs in a small piece of TiO$_2$ film coated on a Mo TEM grid, indicating the existence of Au NPs (marked by the yellow circles) through the entire depth of the TiO$_2$ film.

In order to further investigate the distribution of the Au NPs throughout the thin film, a Mo TEM grid with carbon film was spin-coated with the plasmon-embedded TiO$_2$ sol-gel, which was then calcined and investigated by STEM-HAADF imaging. As the signal of the STEM-HAADF image is approximately proportional to the square of the atomic number Z, the bright Au NPs can easily be distinguished from the surrounding TiO$_2$ film (Figure 8 b). Discrete pieces of the TiO$_2$ film were found on the Mo grid. Some of the TiO$_2$ pieces are not positioned parallel with the Mo grids, but at certain angles with the grid, allowing tilting them to view the cross-section or even the bottom side of the TiO$_2$ pieces. Figure 8b shows a small piece of TiO$_2$ film that has an intersecting angle of 17.7° with the Mo grid. This film was tilted 72.3° to be parallel with the incoming electron-beam, so that a cross-section of the TiO$_2$ film could be imaged. The TiO$_2$ piece is so small that the thickness of this piece in its geometry still allows the penetration of the electron beam, thus enabling the visualisation of the Au

1   NPs. It is clear that there are Au NPs (marked by yellow circles) at different depths throughout the TiO_2

2   film. The nanoparticle size in the 0.5 wt% Au-embedded coating was found to be (16 ± 4) nm, as

3   presented in the histogram Figure S4.

4   Contact angle measurements under dark conditions showed that pure TiO_2 coatings are

5   characterised by a water contact angle of $(15 \pm 2)°$, and for the 0.5 wt% Au-embedded TiO_2 coatings a

6   similar contact angle of $(14 \pm 2)°$ is measured. When comparing this with uncoated Borofloat®

7   substrates with a water contact angle of $(23 \pm 2)°$ and the commercial benchmark PilkingtonActiv™,

8   with a measured water contact angle of $(37 \pm 6)°$, the newly developed coatings are much more

9   wetting. This hydrophilic nature is beneficial for the use of the coating in self-cleaning applications,

10   since a wetting surface can wash off dirt more easily.[48] Titania is known to increase the surface

11   hydrophilicity under UV irradiation.[49,50] This was also measured by means of water contact angles

12   of $(6.9 \pm 0.8)°$ for pure TiO_2, $(5 \pm 2)°$ for 0.5 wt% Au-embedded TiO_2 thin films, making the surfaces

13   superhydrophylic. As a reference, for PilkingtonActiv™ the water contact angle dropped to $(11 \pm 1)°$,

14   while for uncoated Borofloat® there was no significant change $(20 \pm 2)°$, as expected. Therefore, it may

15   be concluded that both under dark and irradiated conditions, the developed coatings are more

16   hydrophilic than the commercial reference sample, and the Au-containing films are slightly more

17   wetting that the pure TiO_2 thin films. Photographs of the water contact angle measurements are

18   provided in Supporting Information Figure S5.

19   **Photocatalytic self-cleaning activity**

20   The photocatalytic activity of the films was evaluated by monitoring the degradation of stearic

21   acid from the surface, a widely applied method for assessing the activity of self-cleaning materials as

22   stearic acid is considered to be an adequate model compound for organic fouling.[1,5,20,38,51] Mills

23   and Wang reported complete mineralisation of stearic acid to CO_2 with reaction intermediates that

24   degrade faster than the original fouling compound for similar sol-gel based titania coatings.[51] The

25   results of our experiments performed under both UVA and simulated solar light are presented in Figure

9. All measurements were performed in triplicate and for the ease of comparison, the relative improvement of the Au-modified films compared to the pristine reference is presented and calculated as the ratio of their respective formal quantum efficiencies (FQEs). Under pure UVA illumination (Figure 9a), it can be seen that embedding gold nanoparticles into TiO_2 causes the photocatalytic activity to increase compared to the unmodified sample (up to 16% for the 3 wt% sample). The large contact interface between the embedded nanoparticles and TiO_2 is thought to improve the electron transfer efficiency from the excited semiconductor to the passive Au nanoparticle electron sinks. Under broadband solar light illumination (Figure 9b) a similar trend can be observed, where higher loadings lead to an increased activity relative to the unmodified sample. The relative improvement starts to saturate around 1 wt%, that can thus be considered to be an adequate loading from a cost-effectiveness point of view. Relative improvements up to 29% and 40% for the 1 wt% and 3 wt% samples, respectively, are achieved. It is clear that these improvements are much higher than the ones observed under pure UVA illumination (Figure 9 a *versus* b) and can therefore not be solely attributed to the UV part of the simulated sunlight. These results therefore support the hypothesis that a synergistic interaction occurs when dually exciting the plasmonic photocatalyst under solar irradiation (*i.e.* simultaneously exciting the semiconductor by UV light and the plasmonic nanoparticles by visible light).
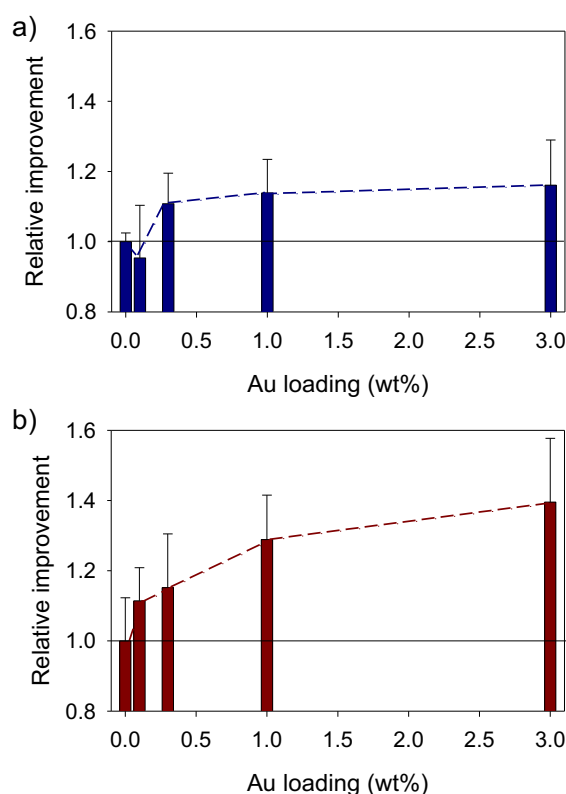
Figure 9. Relative improvement of the embedded Au/TiO$_2$ samples with different loadings with regard to the unmodified thin film under (a) UVA and (b) AM1.5 simulated solar light illumination.

In order to compare the newly proposed method with an alternative available method from literature, samples prepared according to Sonawane *et al*. have also been measured. It is observed that they are less performant than the newly proposed method (Figure 10). The stearic acid degradation rate of the Sonawane non-modified TiO$_2$ coated sample is 3.7×10^{11} molecules cm^{-2} s^{-1}, which is 8% of the non-modified coatings of the proposed method, which reach a stearic acid degradation rate of 4.4×10^{12} molecules cm^{-2} s^{-1}. The addition of gold nanoparticles into the Sonawane sol-gel coatings increases the stearic acid degradation rate 2.5 times to 8.3×10^{11} molecules cm^{-2} s^{-1}, which is still 6 times lower than the proposed method with a rate of 4.9×10^{12} molecules cm^{-2} s^{-1}. When comparing the new coating to the commercial benchmark PilkingtonActiv™ with a stearic acid degradation rate of 6.2×10^{11} molecules cm^{-2} s^{-1}, the pure TiO$_2$ coatings performs 6 times better. The Au-embedded coatings outperform the benchmark by nearly an entire order of magnitude.
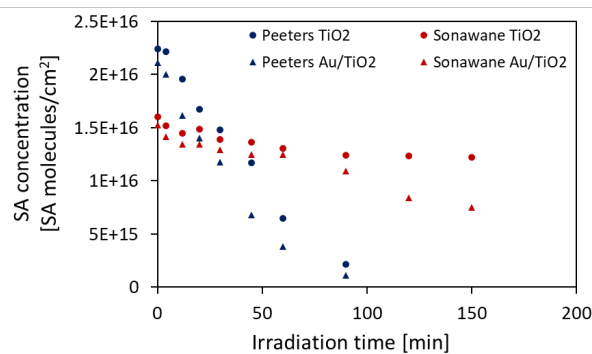
1

Attempts have been made to evaluate the long-term stability of the prepared coatings by re-testing 6-month-old samples. The relative improvement with respect to unmodified samples is well retained, however, a fair one-on-one comparison of the absolute conversion rates could not be made due to large differences in ambient temperature and relative humidity with regard to the initial measurement conditions. Ongoing research focusses on an alternative strategy for evaluating the long-term performance of the coatings under real life conditions, on which we hope to report very soon.

Compared to previous work on a broadband 'rainbow' plasmonic photocatalyst that absorbs light over the entire UV-visible light range,[40] a twice as high efficiency improvement is obtained in this work with the embedded gold nanoparticles. Although the 'rainbow' system was specifically designed to perform well under actual solar light irradiation, an overall improvement of the FQE of 16% was obtained for 1.5 wt% mixed metal loading on the surface of P25, whereas in this work already 29% improvement has been measured for only 1.0 wt% of gold embedded thin films with a much narrower plasmon resonance band. This is a clear indication that the embedment strategy is a promising approach to maximise the interaction area between the photocatalytic support and the plasmonic sensitisers. Improved wavelength tuning of the plasmonic nanostructures to better match with the actual solar radiation spectrum is therefore expected to yield even higher enhancement factors.

4. Conclusion

A convenient strategy to obtain plasmon modified, transparent self-cleaning films based on an *ex-situ* sol-gel synthesis procedure is presented. Gold nanoparticles were prepared according to the Turkevich method, followed by a ligand exchange step to enable a phase transfer from an aqueous colloidal suspension to an organic medium. Finally, the stabilised gold nanoparticles were mixed directly with a titanium precursor during the sol-gel synthesis process, resulting in a one-pot coating suspension containing both the titania source as well as the plasmonic sensitisers. A transparent, smooth, superhydrophylic, homogeneous, anatase phase TiO_2 thin film with the stabilised gold nanostructures embedded in the film matrix and a layer thickness of 94 nm was obtained. A clear red shift of the SPR band was observed for embedded Au nanoparticles (626 nm) compared to the colloidal suspension of PVP stabilised Au nanoparticles (521.5 nm). BEI surface imaging hints towards homogeneously distributed Au nanoparticles throughout the TiO_2 film, which was confirmed by TEM measurements. All prepared films showed an increased efficiency toward stearic acid degradation compared to a pristine TiO_2 reference sample under both UVA and simulated solar light illumination (16% and 40%, respectively, for 3 wt% of embedded gold nanoparticles). The newly developed coatings also showed greater stearic acid degradation efficiency than the current commercial benchmark PilkingtonActiv™ and an alternative Au-embedded sol-gel based TiO_2 coating strategy proposed by Sonawane *et al.* [37] The present study shows that the improvement under simulated solar light cannot be solely attributed the UV part of the illumination spectrum, pointing at a synergistic effect of simultaneously exciting the plasmonic photocatalyst with both the UV and visible light components of solar irradiation. We are hopeful this strategy will facilitate the development of efficient solar light driven photocatalytic thin films for real life self-cleaning applications.

5. Acknowledgements

23

1 **References**

2 [1] Y. Paz, Z. Luo, L. Rabenberg, A. Heller, Photooxidative self-cleaning transparent titanium dioxide

3 films on glass, J. Mater. Res. 10 (1995) 2842–2848. doi:10.1557/JMR.1995.2842.

4 [2] A. Mills, G. Hill, S. Bhopal, I.P. Parkin, S.A. O'Neill, Thick titanium dioxide films for semiconductor

5 photocatalysis, J. Photochem. Photobiol. A Chem. 160 (2003) 185–194.

6 doi:http://dx.doi.org/10.1016/S1010-6030(03)00206-5.

7 [3] E. Allain, S. Besson, C. Durand, M. Moreau, T. Gacoin, J.P. Boilot, Transparent mesoporous

8 nanocomposite films for self-cleaning applications, Adv. Funct. Mater. 17 (2007) 549–554.

9 doi:10.1002/adfm.200600197.

10 [4] P.A. Christensen, T.A. Egerton, S.A.M. Kosa, J.R. Tinlin, K. Scott, The photoelectrocatalytic

11 oxidation of aqueous nitrophenol using a novel reactor, J. Appl. Electrochem. 35 (2005) 683–

12 692. doi:10.1007/s10800-005-1366-8.

13 [5] A. Mills, A. Lepre, N. Elliott, S. Bhopal, I.P. Parkin, S.A. O'Neill, Characterisation of the

14 photocatalyst Pilkington Activ^{TM}: A reference film photocatalyst?, J. Photochem. Photobiol. A

15 Chem. 160 (2003) 213–224. doi:10.1016/S1010-6030(03)00205-3.

16 [6] A. Mills, N. Elliott, I.P. Parkin, S.A. O'Neill, R.J.H. Clark, Novel TiO2 CVD films for semiconductor

17 photocatalysis, J. Photochem. Photobiol. A-Chemistry. 151 (2002) 171–179.

18 [7] J.D. DeLoach, G. Scarel, C.R. Aita, Correlation between titania film structure and near ultraviolet

19 optical absorption, J. Appl. Phys. 85 (1999) 2377–2384. doi:10.1063/1.369553.

20 [8] Gopal K. Mor, Karthik Shankar, Maggie Paulose, A. Oomman K. Varghese, C.A. Grimes, Use of

21 Highly-Ordered TiO2 Nanotube Arrays in Dye-Sensitized Solar Cells, Nano Lett. 6 (2006) 215–

22 218. doi:10.1021/NL052099J.

23 [9] K. Ostrikov, Reactive plasmas as a versatile nanofabrication tool, Rev. Mod. Phys. 77 (2005)

24 489–511. doi:10.1103/RevModPhys.77.489.

[10] S.W. Verbruggen, S. Deng, M. Kurttepeli, D.J. Cott, P.M. Vereecken, S. Bals, J. a. Martens, C. Detavernier, S. Lenaerts, Photocatalytic acetaldehyde oxidation in air using spacious TiO2 films prepared by atomic layer deposition on supported carbonaceous sacrificial templates, Appl. Catal. B Environ. 160–161 (2014) 204–210. doi:10.1016/j.apcatb.2014.05.029.

[11] S. Deng, S.W. Verbruggen, S. Lenaerts, J.A. Martens, S. Van Den Berghe, K. Devloo-Casier, W. Devulder, J. Dendooven, D. Deduytsche, C. Detavernier, Controllable nitrogen doping in as deposited TiO2 film and its effect on post deposition annealing, J. Vac. Sci. Technol. A Vacuum, Surfaces Film. 32 (2014). doi:10.1116/1.4847976.

[12] S.W. Verbruggen, TiO2 photocatalysis for the degradation of pollutants in gas phase: From morphological design to plasmonic enhancement, J. Photochem. Photobiol. C Photochem. Rev. 24 (2015) 64–82. doi:10.1016/j.jphotochemrev.2015.07.001.

[13] M. Pelaez, N.T. Nolan, S.C. Pillai, M.K. Seery, P. Falaras, A.G. Kontos, P.S.M. Dunlop, J.W.J. Hamilton, J.A. Byrne, K.O. Shea, M.H. Entezari, D.D. Dionysiou, A review on the visible light active titanium dioxide photocatalysts for environmental applications, Appl. Catal. B, Environ. 125 (2012) 331–349. doi:10.1016/j.apcatb.2012.05.036.

[14] D. Wang, S.C. Pillai, S.H. Ho, J. Zeng, Y. Li, D.D. Dionysiou, Plasmonic-based nanomaterials for environmental remediation, Appl. Catal. B Environ. 237 (2018) 721–741. doi:10.1016/j.apcatb.2018.05.094.

[15] D.B. Ingram, S. Linic, Water Splitting on Composite Plasmonic-Metal/Semiconductor Photoelectrodes: Evidence for Selective Plasmon-Induced Formation of Charge Carriers near the Semiconductor Surface, J. Am. Chem. Soc. 133 (2011) 5202–5205. doi:10.1021/ja200086g.

[16] D.B. Ingram, P. Christopher, J.L. Bauer, S. Linic, Predictive Model for the Design of Plasmonic Metal/Semiconductor Composite Photocatalysts, Acs Catal. 1 (2011) 1441–1447.

[17] E. Kowalska, O.O.P. Mahaney, R. Abe, B. Ohtani, Visible-light-induced photocatalysis through surface plasmon excitation of gold on titania surfaces, Phys. Chem. Chem. Phys. 12 (2010)

1   2344–2355.

2   [18]   E. Kowalska, R. Abe, B. Ohtani, Visible light-induced photocatalytic reaction of gold-modified

3   titanium(iv) oxide particles: action spectrum analysis, Chem. Commun. 0 (2009) 241–243.

4   doi:10.1039/B815679D.

5   [19]   A. Tanaka, A. Ogino, M. Iwaki, K. Hashimoto, A. Ohnuma, F. Amano, B. Ohtani, H. Kominami,

6   Gold-Titanium(IV) Oxide Plasmonic Photocatalysts Prepared by a Colloid-Photodeposition

7   Method: Correlation Between Physical Properties and Photocatalytic Activities, Langmuir. 28

8   (2012) 13105–13111.

9   [20]   S.W. Verbruggen, M. Keulemans, M. Filippousi, D. Flahaut, G. Van Tendeloo, S. Lacombe, J.A.

10   Martens, S. Lenaerts, Plasmonic gold–silver alloy on TiO2 photocatalysts with tunable visible

11   light   activity,   Appl.   Catal.   B   Environ.   156–157   (2014)   116–121.

12   doi:http://dx.doi.org/10.1016/j.apcatb.2014.03.027.

13   [21]   N. Blommaerts, R. Asapu, N. Claes, S. Bals, S. Lenaerts, S.W. Verbruggen, Gas phase

14   photocatalytic spiral reactor for fast and efficient pollutant degradation, Chem. Eng. J. 316

15   (2017). doi:10.1016/j.cej.2017.02.038.

16   [22]   R. Asapu, N. Claes, S. Bals, S. Denys, C. Detavernier, S. Lenaerts, S.W. Verbruggen, Silver-

17   polymer core-shell nanoparticles for ultrastable plasmon-enhanced photocatalysis, Appl. Catal.

18   B Environ. 200 (2017) 31–38. doi:10.1016/j.apcatb.2016.06.062.

19   [23]   A. Naldoni, M. D'Arienzo, M. Altomare, M. Marelli, R. Scotti, F. Morazzoni, E. Selli, V. Dal Santo,

20   Pt and Au/TiO2 photocatalysts for methanol reforming: Role of metal nanoparticles in tuning

21   charge trapping properties and photoefficiency, Appl. Catal. B Environ. 130–131 (2013) 239–

22   248. doi:10.1016/j.apcatb.2012.11.006.

23   [24]   I. Caretti, M. Keulemans, S.W. Verbruggen, S. Lenaerts, S. Van Doorslaer, Light-Induced

24   Processes in Plasmonic Gold/TiO2 Photocatalysts Studied by Electron Paramagnetic Resonance,

25   Top. Catal. 58 (2015) 776–782. doi:10.1007/s11244-015-0419-4.

[25] J.B. Priebe, M. Karnahl, H. Junge, M. Beller, D. Hollmann, A. Brückner, Water reduction with visible light: synergy between optical transitions and electron transfer in Au-TiO(2) catalysts visualized by in situ EPR spectroscopy., Angew. Chem. Int. Ed. Engl. 52 (2013) 11420–4. doi:10.1002/anie.201306504.

[26] R. Asapu, N. Claes, R.-G. Ciocarlan, M. Minjauw, C. Detavernier, P. Cool, S. Bals, S.W. Verbruggen, Electron Transfer and Near-Field Mechanisms in Plasmonic Gold-Nanoparticle-Modified TiO $_2$ Photocatalytic Systems, ACS Appl. Nano Mater. (2019) acsanm.9b00485. doi:10.1021/acsanm.9b00485.

[27] R. Asapu, R. Ciocarlan, N. Claes, N. Blommaerts, M. Minjauw, T. Ahmad, J. Dendooven, P. Cool, S. Bals, S. Denys, C. Detavernier, S. Lenaerts, S.W. Verbruggen, Plasmonic near-field localization of silver core-shell nanoparticle assemblies via wet chemistry nanogap engineering, ACS Appl. Mater. Interfaces. 9 (2017) 41577–41585.

[28] X.-C. Ma, Y. Dai, L. Yu, B.-B. Huang, Energy transfer in plasmonic photocatalytic composites, Light Sci. Appl. 5 (2016) e16017. doi:10.1038/lsa.2016.17.

[29] M.W. Knight, Y. Wang, A. Urban, A. Sobhani, B. Zheng, P. Nordlander, N.J. Halas, Embedding Plasmonic Nanostructure-diodes enhances Hot Electron Emission, Nano Lett. 13 (2013) 1687–1692. doi:10.1021/nl400196z.

[30] A. Primo, A. Corma, H. García, Titania supported gold nanoparticles as photocatalyst., Phys. Chem. Chem. Phys. 13 (2011) 886–910. doi:10.1039/c0cp00917b.

[31] C. Fang, H. Jia, S. Chang, Q. Ruan, P. Wang, T. Chen, J. Wang, (Gold core)/(titania shell) nanostructures for plasmon-enhanced photon harvesting and generation of reactive oxygen species, Energy Environ. Sci. 7 (2014) 3431–3438. doi:10.1039/C4EE01787K.

[32] S. Pradhan, D. Ghosh, S. Chen, Janus nanostructures based on Au-TiO2 heterodimers and their photocatalytic activity in the oxidation of methanol, ACS Appl. Mater. Interfaces. 1 (2009) 2060–2065. doi:10.1021/am900425v.

1 [33] D. Buso, J. Pacifico, A. Martucci, P. Mulvaney, Gold-nanoparticle-doped TiO2 semiconductor

2   thin films: Optical characterization, Adv. Funct. Mater. 17 (2007) 347–354.

3   doi:10.1002/adfm.200600349.

4 [34] Y. Xie, K. Ding, Z. Liu, R. Tao, Z. Sun, H. Zhang, G. An, In Situ Controllable Loading of Ultra ne

5   Noble Metal Particles on Titania, (2009) 6648–6649.

6 [35] P. Wang, T.F. Xie, H.Y. Li, L. Peng, Y. Zhang, T.S. Wu, S. Pang, Y.F. Zhao, D.J. Wang, Synthesis and

7   plasmon-induced charge-transfer properties of monodisperse gold-doped titania

8   microspheres, Chem. - A Eur. J. 15 (2009) 4366–4372. doi:10.1002/chem.200802138.

9 [36] L.M. Liz-Marzan, Tailoring surface plasmons through the morphology and assembly of metal

10   nanoparticles, Langmuir. 22 (2006) 32–41.

11 [37] R.S. Sonawane, M.K. Dongare, Sol – gel synthesis of Au/TiO2 thin films for photocatalytic

12   degradation of phenol in sunlight, J. Mol. Catal. A Chem. 243 (2006) 68–76.

13   doi:10.1016/j.molcata.2005.07.043.

14 [38] M.N. Ghazzal, N. Barthen, N. Chaoui, Photodegradation kinetics of stearic acid on UV-irradiated

15   titania thin film separately followed by optical microscopy and Fourier transform infrared

16   spectroscopy, Appl. Catal. B Environ. 103 (2011) 85–90.

17 [39] J. Turkevich, P.C. Stevenson, J. Hillier, A study of the nucleation and growth processes in the

18   synthesis of colloidal gold, Discuss. Faraday Soc. 11 (1951) 55–75.

19 [40] S.W. Verbruggen, M. Keulemans, B. Goris, N. Blommaerts, S. Bals, J.A. Martens, S. Lenaerts,

20   Plasmonic 'rainbow' photocatalyst with broadband solar light response for environmental

21   applications, Appl. Catal. B Environ. 188 (2016) 147–153. doi:10.1016/j.apcatb.2016.02.002.

22 [41] C. Graf, D.L.J. Vossen, A. Imhof, A. Van Blaaderen, A general method to coat colloidal particles

23   with silica, Langmuir. 19 (2003) 6693–6700. doi:10.1021/la0347859.

24 [42] M. Tejamaya, I. Römer, R.C. Merrifield, J.R. Lead, Stability of citrate, PVP, and PEG coated silver

nanoparticles in ecotoxicology media, Environ. Sci. Technol. 46 (2012) 7011–7017. doi:10.1021/es2038596.

[43] J. Yang, J.Y. Lee, J.Y. Ying, Phase transfer and its applications in nanotechnology, Chem. Soc. Rev. 40 (2011) 1672–1696. doi:10.1039/B916790K.

[44] N.G. Bastús, F. Merkoçi, J. Piella, V. Puntes, Synthesis of highly monodisperse citrate-stabilized silver nanoparticles of up to 200 nm: Kinetic control and catalytic properties, Chem. Mater. 26 (2014) 2836–2846. doi:10.1021/cm500316k.

[45] J. Zhang, Q. Xu, Z. Feng, M. Li, C. Li, Importance of the relationship between surface phases and photocatalytic activity of TiO2, Angew. Chemie - Int. Ed. 47 (2008) 1766–1769. doi:10.1002/anie.200704788.

[46] S. Deng, S.W. Verbruggen, Z. He, D.J. Cott, P.M. Vereecken, J.A. Martens, S. Bals, S. Lenaerts, C. Detavernier, Atomic layer deposition-based synthesis of photoactive TiO2 nanoparticle chains by using carbon nanotubes as sacrificial templates, RSC Adv. 4 (2014) 11648–11653. doi:10.1039/c3ra42928h.

[47] G. Naudin, D.R. Ceratti, M. Faustini, Sol-Gel Derived Functional Coatings for Optics, in: 2017: pp. 61–99. doi:10.1007/978-3-319-50144-4_3.

[48] D. Enea, M. Bellardita, P. Scalisi, G. Alaimo, L. Palmisano, Effects of weathering on the performance of self-cleaning photocatalytic paints, Cem. Concr. Compos. 96 (2019) 77–86. doi:10.1016/j.cemconcomp.2018.11.013.

[49] S. Banerjee, D.D. Dionysiou, S.C. Pillai, Self-cleaning applications of TiO$_2$ by photo-induced hydrophilicity and photocatalysis, Appl. Catal. B Environ. 176–177 (2015) 396–428. doi:10.1016/j.apcatb.2015.03.058.

[50] R. Wang, K. Hashimoto, A. Fujishima, M. Chikuni, E. Kojima, A. Kitamura, M. Shimohigoshi, T. Watanabe, Light-induced amphiphilic surfaces [4], Nature. 388 (1997) 431–432. doi:10.1038/41233.

1   [51]   A. Mills, J. Wang, Simultaneous monitoring of the destruction of stearic acid and generation of

2   carbon dioxide by self-cleaning semiconductor photocatalytic films, J. Photochem. Photobiol. A

3   Chem. 182 (2006) 181–186. doi:10.1016/j.jphotochem.2006.02.010.

4